# Low-energy structures in strong-field ionization

I. A. Ivanov,[1,2,*] Chang Hee Nam,[1,3] and Kyung Taec Kim[1,3,†]

[1]*Center for Relativistic Laser Science, Institute for Basic Science, Gwangju 500-712, Republic of Korea*

[2]*Research School of Physics and Engineering, The Australian National University, Canberra ACT 0200, Australia*

[3]*Advanced Photonics Research Institute, GIST, Gwangju 500-712, Republic of Korea*

(Received 28 January 2016; revised manuscript received 14 March 2016; published 4 April 2016)

We show that the Gabor transform provides a convenient tool allowing one to study the origin of the low-energy structures (LES) in the process of the strong-field ionization. The classical trajectories associated with the stationary points of the Gabor transform enable us to explicate the role of the forward scattering process in forming LES. Our approach offers a fully quantum mechanical description of LES, which can also be applied for other strong-field processes.

DOI: 10.1103/PhysRevA.93.043404

## I. INTRODUCTION

The standard picture of the strong-field ionization is based on the so-called Keldysh-Faisal-Reiss (KFR) or strong-field approximation (SFA) theory [1–3] and its subsequent modifications [4–10]. For small values of the Keldysh parameter $\gamma = \omega\sqrt{2|\varepsilon_0|}/E$ ($\omega$, $E$, and $|\varepsilon_0|$ are the frequency, field strength, and ionization potential of the target system expressed in atomic units) the electron energy spectrum, according to the KFR, exhibits a plateau extending up to the energies of $2U_p$ (here $U_p = E^2/4\omega^2$ is the ponderomotive energy). This plateau is formed by the so-called "direct" electrons called so because KFR in the original form does not take into account effect of the ionic core on the electron motion after the ionization event. For electron energies exceeding $2U_p$ a second plateau extending up to the energies of $10U_p$ can be seen in the electron energy spectra. This plateau is due to the interaction of electrons with the ionic core. The SFA can be generalized to include these effects by considering the electron-ion core interaction as a perturbation [11,12]. These features of the electron spectra can also be understood using the so-called simple-man model (SMM) [13] in which electrons can emerge into the continuum at different times during the laser pulse (typically with zero velocities in the pulse polarization direction), their subsequent motion in the laser field being described entirely classically.

As far as small energy region is concerned, the SFA predicts that for values of the Keldysh parameter momentum and energy distributions of the ionized electron should be smooth functions of electron momentum and energy exhibiting little structure [5]. Experimental discovery of the low-energy structures (LES) [14] in the electron spectra for energies of the order of a fraction of the ponderomotive energy $U_p = E^2/4\omega^2$ was, therefore, dubbed an "ionization surprise" [15]. The LES were found to be present in the spectra of different atomic targets [14] indicating that they are a general phenomenon. The LES have also been found to disappear with growing ellipticity of the driving laser pulse [14,16] which led to a suggestion that a rescattering process, the probability of which is heavily damped for the nonlinearly polarized pulses, might be somehow responsible for the origin of the LES [15].

A semiclassical approach based on quantum orbits has been presented in [17]. It was shown [17] that the LES can be attributed to a forward scattering process, a type of the rescattering event in which electron upon ionization moves first in the direction opposite to the detector, subsequently turns back, returns to the ionic core, and moves in the direction of the detector. A detailed analysis of the classical orbits of the SMM presented in [18] showed that essential physics of the LES can be explained on the basis of this model. The work [18] also reports results of the quantum orbits analysis using the improved SFA taking into account effects of the electron-core interaction, with the conclusion that the forward scattering process is responsible for the LES.

It is well known that the strong Coulomb interaction can considerably alter the SFA-based picture of ionization for linearly or near linearly polarized laser pulses. The Coulomb focusing effect, for example, is responsible for the appearance of a cusp [19] at zero momenta in the lateral momentum distribution (i.e., the distribution of the momenta in the plane perpendicular to the polarization vector). The same effect is responsible for a considerable deviation of the experimental results [20] from the SFA-based theoretical predictions for the location of the peak of the electron momentum distribution in the polarization plane of the driving pulse with low ellipticity. These phenomena vanish with growing ellipticity of the driving laser pulse [20,21], when electron cannot return to the ionic core. Coulomb focusing, therefore, is caused ultimately by the Coulomb field of the ionic core at the small distances. Physics of the LES appears to be different. It was found [22] that the LES are very sensitive to minor modifications of the long-range tail of the Coulomb potential of the ion. Authors of this work found that replacing the Coulomb ionic potential with the Yukawa potential with even a small scaling parameter leads to disappearance of the LES. It is the Coulomb attraction between the electron and ionic core at the large distances which seems to be responsible for the origin of the LES [22]. This view is compatible with the conclusions made in [18], where the connection between the forward-scattering process and the LES was explained by noting that the Coulomb forward-scattering amplitude which is proportional to $q^{-2}$ (here $\boldsymbol{q}$ is the momentum transferred to the core) diverges for $\boldsymbol{q} \to 0$, which makes the contribution of the electrons which

*Igor.Ivanov@anu.edu.au

†kyungtaec@gist.ac.kr

 

underwent the forward scattering rise above the contribution of the direct electrons. This leads ultimately to the domination of the LES in the low-energy region of the spectrum. This divergent behavior of the scattering amplitude is due to the long-range tail of the Coulomb potential and is absent for the Yukawa potential.

The methods used in [17,18] rely on the use of the classical or quantum orbits. Quantum orbits are solutions (generally complex) of the equations resulting from application of the saddle-point method to the evaluation of the SFA or improved SFA expressions for the ionization amplitudes. Classical orbits are essentially their real parts. The reason why these approaches are so helpful is their ability to produce results which allow simple interpretation and understanding of the underlying physics. A rigorous analysis of light-matter interactions should be based on a quantum mechanical approach which consists in describing evolution of a wave function by solving the time-dependent Schrödinger equation. It is, however, often difficult to interpret the result of the numerical experiment due to the wave nature of the solution. Classical trajectory of the particle, on the other hand, offers straightforward interpretation. Here, we introduce a technique which links classical trajectories of the electron in the strong laser field and certain properties of the Gabor transform of the wave function. We apply this technique to analyze the origin of LES in photoelectron spectra. This approach allows us to explicate the origin of LES using results obtained from the fully *ab initio* quantum mechanical calculation.

## II. THEORY AND RESULTS

As a model we consider the hydrogen atom. The laser pulse is linearly polarized along the $z$ direction, which we use as a quantization axis:

$$E_z = E_0 f(t) \cos \omega t, \tag{1}$$

and has the following parameters: carrier frequency $\omega = 0.015$ a.u. (3 $\mu$w wavelength) and peak pulse strength $E_0 = 0.05$ a.u. (intensity of $8.77 \times 10^{13}$ W/cm$^2$). The pulse envelope is a Gaussian: $f(t) = \exp\{\frac{-2 \ln 2 (t-t_m)^2}{\tau^2}\}$, where $\tau = 14.5$ fs (FWHM of the pulse). Laser field is present on a time interval $(0, T_1)$, where $T_1 = 10T$, $T = 2\pi/\omega$ (optical cycle of the field), and $t_m = T_1/2$ (midpoint of the pulse). The field is shown in Fig. 1.

To solve the TDSE we employed the procedure described in the works [21,23]. Atom-field interaction is described using the velocity gauge. Solution of the TDSE is represented as a series in spherical harmonics:

$$\Psi(\boldsymbol{r},t) = \sum_{l=0}^{l_{\max}} f_l(r,t) Y_{l0}(\theta). \tag{2}$$

The radial part of the TDSE is discretized on the grid with the step size $\delta r = 0.1$ a.u. in a box of the size $R_{\max} = 2000$ a.u. We used $l_{\max} = 100$ in the calculations reported below. Solution of the TDSE is propagated in time using the matrix iteration method [24]. Electron spectra are obtained by projecting solution of the TDSE at the end of the pulse on the set of the scattering states of the hydrogen atom satisfying ingoing boundary conditions. In the deep tunneling

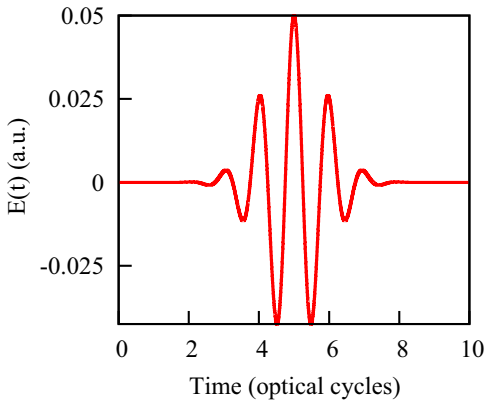


FIG. 1. Electric field of the laser pulse.

regime we consider (the Keldysh parameter $\gamma \approx 0.3$ for the field parameters we employ) convergence of the partial wave expansion (2) can be notoriously slow [24]. The necessary checks ensuring that convergence has been achieved have been performed. In Fig. 2 we give an illustration of the convergence of the results with respect to the variation of parameter $l_{\max}$.

The calculated spectra for $l_{\max} = 80$ and $l_{\max} = 100$ are virtually identical, which motivated our choice of $l_{\max} = 100$ for the calculations reported below. The angle integrated energy spectrum for a wider energy interval and the low-energy part of the spectrum containing the LES are shown in Fig. 3.

LES are clearly visible in the angle integrated spectrum. For the study of LES angle-resolved characteristics are more informative. We shall be interested below in electron spectra in the forward (positive $z$) and backward (negative $z$ directions). These spectra are shown in Fig. 4. To elucidate the origin of the LES we performed a numerical experiment with the solution of the TDSE. As we mentioned above, the *ab initio* spectra are obtained by projecting the TDSE solution on the set of the hydrogen scattering states. We may try to gauge the relative importance of different regions of the electron's configuration space by putting the TDSE wave function to zero for different intervals of the radial variable $r$. Results are shown in Fig. 4. As one can see, the region of the radial variable $r \in (100,200)$ a.u. is particularly important for forming LES. If the wave

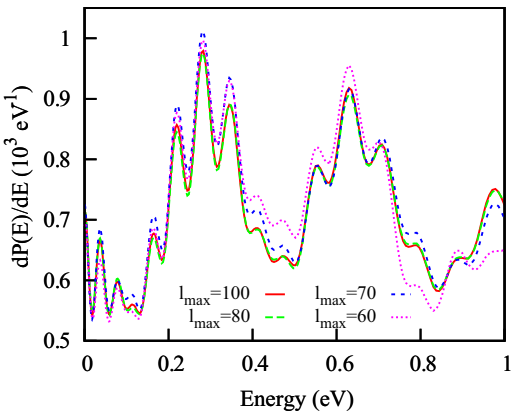


FIG. 2. Convergence of the results for the angle integrated electron energy spectrum with respect to the parameter $l_{\max}$.

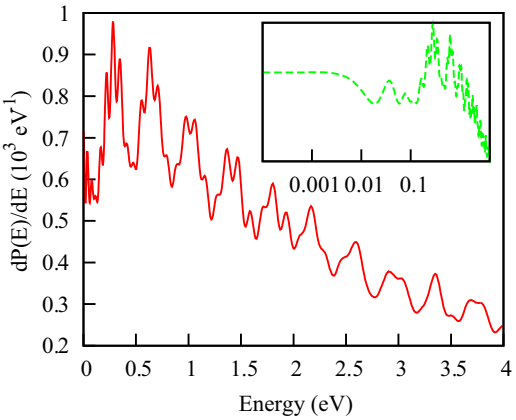


FIG. 3. Angle integrated electron energy spectrum for hydrogen atom ionized by the laser pulse (1). Inset magnifies on the low-energy region of the spectrum below 1 eV.

function at the end of the pulse is forced to be zero inside this interval LES almost completely disappear.

To understand why it happens we will take a closer look at the structure of the wave function describing the ionization process. More specifically, we will analyze the wave function describing the system at the moment $t = T_1$ corresponding to the end of the laser pulse. A better insight can be obtained if we

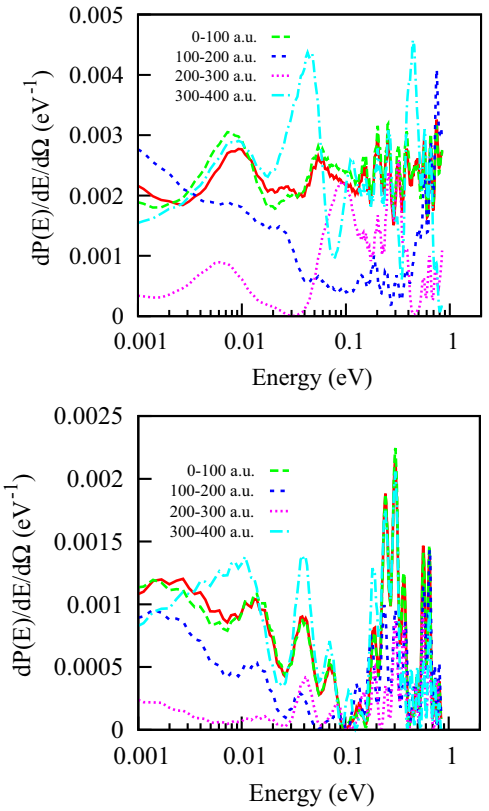


FIG. 4. (Top panel) Solid (red) line: forward ionization probability as a function of electron energy. Also shown are the results obtained by putting the TDSE wave function to zero in different intervals (as indicated in the legend) of radial variable $r$. (Bottom panel) The same for the ionization probability in backward direction.

express the information contained in the wave function in terms of the quantities allowing simple physical interpretation, such as states with (almost) well-defined positions and momenta. This can be achieved by means of the Gabor transform [25–28] (also called the windowed Fourier transform). This transform and closely related wavelet transforms can be used if one wishes to obtain information about behavior of a function in the domains corresponding to conjugate variables. This pair of the conjugate variables can be chosen as time and frequency, for example, as it was done in [28,29], where Gabor transform was used to study properties of the high harmonics emission both in time and frequency domains. In [29] the Gabor transform was applied to the dipole acceleration signal obtained by solving numerically the TDSE. This allowed a representation of the harmonic intensity as a function of both time and frequency. Concentrating on a frequency interval corresponding to a given harmonic order it is possible then to study temporal characteristics of the high harmonic generation process, such as ionization and emission times [29].

We shall be interested below in another pair of conjugate variables—position and momentum. To define the Gabor transform in this case one should choose a square integrable function $\Phi(\boldsymbol{r})$ normalized to 1 (a window function, to be specified below), from which a set of the so-called daughter functions $\Phi_{\boldsymbol{R}\boldsymbol{p}}(\boldsymbol{r}) = \Phi(\boldsymbol{r} - \boldsymbol{R})e^{i\boldsymbol{p}\cdot\boldsymbol{r}}$ (with all possible pairs $\boldsymbol{R}, \boldsymbol{p}$) can be obtained. Gabor transform of a square integrable function $f(\boldsymbol{r})$ is then

$$T(\boldsymbol{R}, \boldsymbol{p}) = \int \Phi^*_{\boldsymbol{R}\boldsymbol{p}}(\boldsymbol{r}) f(\boldsymbol{r})\, d\boldsymbol{r}. \tag{3}$$

The set of $\Phi_{\boldsymbol{R}\boldsymbol{p}}(\boldsymbol{r})$ with all possible pairs of the real of $\boldsymbol{R}$ and $\boldsymbol{p}$ forms a complete basis set [it is, in fact, an overcomplete set, since there are subsets of all possible pairs $(\boldsymbol{R}, \boldsymbol{p})$ for which $\Phi_{\boldsymbol{R}\boldsymbol{p}}(\boldsymbol{r})$ also form complete basis sets], which means that transform (3) can be inverted. The square-integrable $f(\boldsymbol{r})$ can be reconstructed from the coefficients of its Gabor transform (3) as

$$f(\boldsymbol{r}) = \int T(\boldsymbol{R}, \boldsymbol{p}) \Phi_{\boldsymbol{R}\boldsymbol{p}}(\boldsymbol{r}) d\boldsymbol{R}\, d\boldsymbol{p}, \tag{4}$$

where the coefficients $T(\boldsymbol{R}, \boldsymbol{p})$ are defined in Eq. (3). An easy way to see this is by noting that for the set of the daughter functions $\Phi_{\boldsymbol{R}\boldsymbol{p}}(\boldsymbol{r})$ generated from the window function $\Phi(\boldsymbol{r})$, the closure relation $\int \Phi^*_{\boldsymbol{R}\boldsymbol{p}}(\boldsymbol{r}_1)\Phi_{\boldsymbol{R}\boldsymbol{p}}(\boldsymbol{r}_2)\, d\boldsymbol{R}\, d\boldsymbol{p} = \delta(\boldsymbol{r}_1 - \boldsymbol{r}_2)$ holds.

We will apply the Gabor transform below to the function $f(\boldsymbol{r}) = \Psi(\boldsymbol{r}, T_1)$—the wave function taken at the moment of time corresponding to the end of the pulse. As a window function $\Phi(\boldsymbol{r})$ we choose, following Goldberger and Watson [30], a Gaussian function $\Phi(\boldsymbol{r}) = N e^{-a^2 r^2}$, where normalization coefficient $N = (2a^2/\pi)^{\frac{3}{4}}$. The Gaussian window function is often used in applications of the Gabor transform for the time-frequency analysis, so the transform used in the present work and the one used in [29], for example, are mathematically equivalent with the difference that we are interested in the coordinate-momentum pair of variables. Parameter $a$ in the Gaussian defines the spatial and momentum resolution. We use below the value $a = 0.001$. For the particular value of the parameter $a$ we use, a daughter function $\Phi_{\boldsymbol{R}\boldsymbol{p}}(\boldsymbol{r})$ will describe a wave packet centered around values $\boldsymbol{R}$ and $\boldsymbol{p}$ in

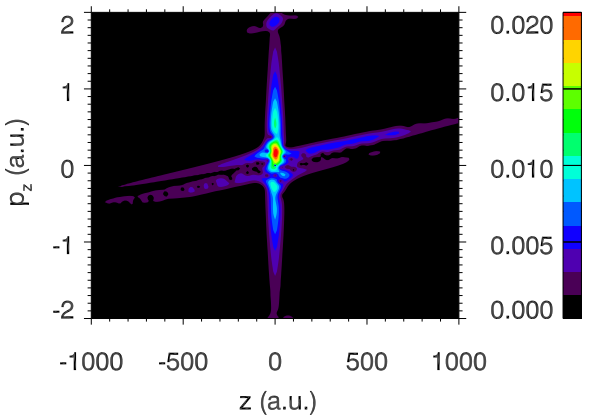


FIG. 5. Amplitude of Gabor transform at the end of the laser pulse for position and momentum vectors $\boldsymbol{R}$ and $\boldsymbol{p}$ in Eq. (4) along the polarization axis.

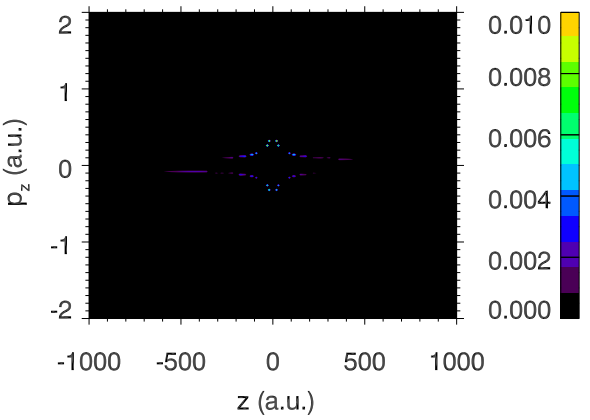


FIG. 6. Amplitude of the Gabor transform at the end of the laser pulse for position and momentum vectors $\boldsymbol{R}$ and $\boldsymbol{p}$ in Eq. (4) along the polarization axis and electron energies $E_{\rm tot} = \boldsymbol{p}^2/2 - 1/R$ satisfying $0 < E_{\rm tot} < 0.05$ eV.

coordinate and momentum spaces, respectively, with spreads of approximately 30 a.u. in coordinate and 0.03 a.u. in momentum space.

The Gabor transform (4) represents wave function at the end of the pulse as a superposition of wave packets with expectation values of coordinate $\boldsymbol{R}$ and momentum $\boldsymbol{p}$. This makes transition to classical description quite transparent. The full six-dimensional Gabor transform as defined in Eq. (4) is, of course, rather time consuming to calculate. Moreover, the results of such a calculation may not be easy to visualize and interpret. We know, however [16,22], that low angular momenta are responsible for the LES structures. Therefore, we may hope that restricting our consideration to the motion along $z$ axis only will capture all the essential physics of the process. In Fig. 5 we show amplitude of the Gabor transform of the wave function at the end of the pulse with position and momentum vectors $\boldsymbol{R}$ and $\boldsymbol{p}$ in Eq. (4) along the polarization axis. This figure can be regarded as a map providing relative probabilities of electron occupying different regions of the phase space at the moment of time corresponding to the end of the pulse. This information can be used, for example, for subsequent classical simulations.

We are interested in the low-energy electrons. A slice showing amplitude of the Gabor transform with total energies $E_{\rm tot} = \boldsymbol{p}^2/2 - 1/R$ satisfying $0 < E_{\rm tot} < 0.05$ eV is shown in Fig. 6.

The points of the phase space corresponding to the energies smaller than 0.05 eV shown in the Fig. 6 appear to have approximately similar probability densities, so at first glance it is unclear how this result can be reconciled with the fact of the importance of the region 100 a.u. $< r <$ 200 a.u. in forming the LES structures which we noticed above. This fact can be accounted for by observing that the Gabor transform is a complex quantity, and information about its phase is equally important. In Fig. 7 we show amplitude and phase of the Gabor transform for total electron energy of 0.01 eV as a function of the $z$ coordinate of the electron. As before, we consider only the transform with $\boldsymbol{R}$ and $\boldsymbol{p}$ in Eq. (4) along the $z$ axis. For a given $z$ value the momentum is found from the energy conservation equation $p_z = \pm\sqrt{2(E_{\rm tot} + 1/|z|)}$, where $E_{\rm tot} = 0.01$ eV.

Figure 7 shows that the phase of the Gabor transform is, generally, a rapidly oscillating function of $z$. The main contributions to the integral (4) defining the inverse Gabor transform comes from the stationary points of the phase. Consider first the case of the positive $p_z$ (top panel of the Fig. 7). As one can see from the figure, there is a stationary point of the phase for the negative value of $z_s^- \approx -190$ a.u. (more exact value which analysis of the numerical data gives is $z_s^- \approx -192.5$ a.u.).

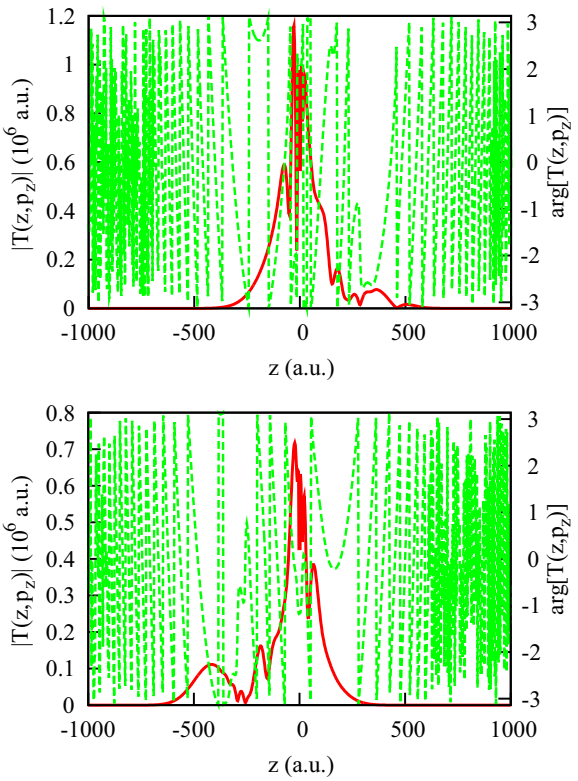


FIG. 7. Amplitude [solid (red) line] and phase [dash (green) line] of the Gabor transform $T(z, p_z)$ for total electron energy of 0.01 eV as function of the $z$ coordinate of the electron's wave packet. Momentum $p_z = \sqrt{2(E_{\rm tot} + 1/|z|)}$ (top panel); $p_z = -\sqrt{2(E_{\rm tot} + 1/|z|)}$ (bottom panel). Total electron energy $E_{\rm tot} = 0.01$ eV.

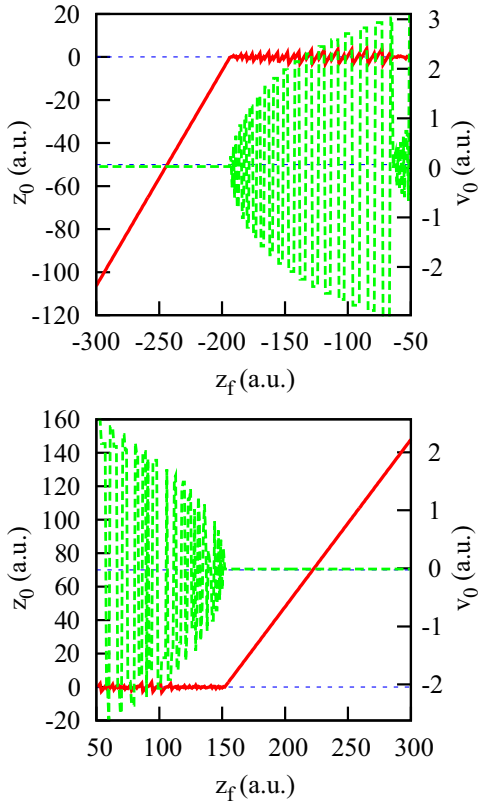


FIG. 8. Dependence of $z_0$ [solid (red) line] and $v_0$ [dash (green) line] on the value of the $z$ coordinate at the moment $t = T_1$ at the end of the laser pulse. Value of the velocity at this moment is such that the total energy $E_{\rm tot} = 0.01$ eV and is positive for the top panel and negative for the bottom panel.

A connection can be established between the stationary point $z_s^- \approx -192.5$ a.u. of the Gabor transform which we have just found and a certain classical electron trajectory. We shall be interested in the classical trajectories used in the SMM to represent the motion of the ionized electron. Such a trajectory is launched at some moment of time (the moment of ionization) from the origin with zero velocity. Let us consider a slightly different problem. Suppose at the moment of time $T_1$ corresponding to the end of the pulse we have an electron at some point $z_f$ on the negative $z$ axis with positive velocity $v_f$ chosen such that total electron energy $E_{\rm tot} = 0.01$ eV. Using these values as initial (or rather final) conditions we propagate classical equations of motion backward in time. We consider one-dimensional classical propagation considering only motion in the $z$ coordinate for an electron in the electric field shown in Fig. 1. Let for each trajectory $z_0$ be the value of the $z$ coordinate at the moment of the closest approach of the trajectory to the origin. Let $v_0$ be the velocity at this moment of time. The dependence of $v_0$ and $z_0$ on $z_f$ (with $v_f$ remaining positive and fixed by energy conservation) is shown in the top panel of Fig. 8.

In the spirit of the SMM we should be looking for a trajectory passing through the point $z = 0$ with near zero velocity. In other words, the classical trajectory describing ionization is the trajectory with the smallest $|v_0|$ and $|z_0|$. As one can see from the illustration in the top panel of the Fig. 8, there is essentially unique trajectory satisfying these

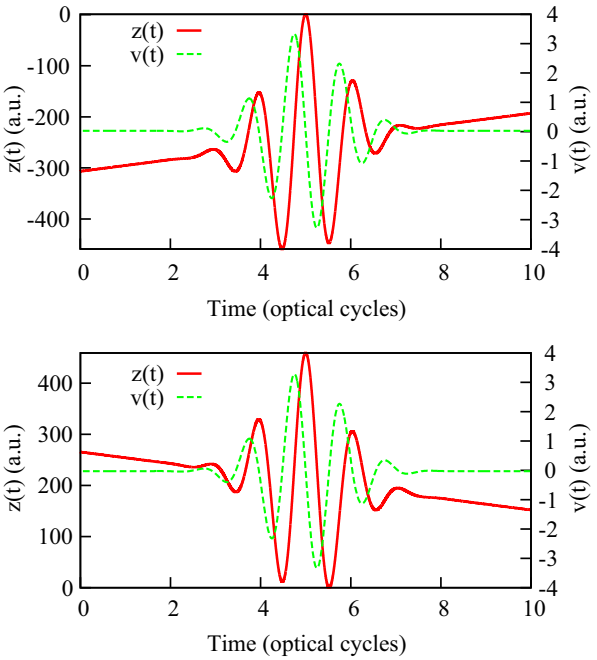


FIG. 9. Classical trajectories originating at the end of the pulse $t = T_1$ from the stationary points of the Gabor transform $z_s^- = -192.5$ a.u. (top panel) and $z_s^+ = 155$ a.u. (bottom panel). The velocity at the moment $T_1$ is fixed by energy conservation so that $E_{\rm tot} = 0.01$ eV and is positive for $z_s^- < 0$ and negative for $z_s^- > 0$.

requirements. For negative $z_f$ the returning trajectories exist only for $z_f$ exceeding certain critical value $z_f^- \approx -193$ for which $v_0$ and $z_0$ have zero values. With further increase of $z_f$ the absolute value of the velocity $v_0$ at the moment of the closest approach grows fast. Trajectories with nonzero velocity at the moment of ionization are exponentially damped [5] and are not considered in the SMM. We are left therefore with the unique classical trajectory which starts at the moment $T_1$ at the point $z_f^- \approx -193$ a.u., which agrees very well with the value of the stationary point of the Gabor transform $z_s^- \approx -192.5$ a.u. we gave above.

For the negative momenta $p_z$ (bottom panel of the Fig. 7) we obtain for the stationary point of the Gabor transform $z_s^+ \approx 155$ a.u. Repeating the classical procedure we described above we find again a unique trajectory starting at the moment of time $t = T_1$ from the point in the phase space with some positive $z_0$ and negative $v_0$ such that $|v_0|$ and $|z_0|$ have the smallest possible values. This is illustrated in the bottom panel of the Fig. 8. Initial (or rather final) $z$ value for this trajectory is $z_f^+ \approx 152$. Again, we have $z_f^+ \approx z_s^+$ with good accuracy.

We surmise thus that the classical trajectories used in the SMM reveal themselves unambiguously as the stationary points of the Gabor transform of the wave function. The trajectories themselves are shown in Fig. 9.

It is, of course, meaningful to follow these trajectories in the past direction only till the moment $t_0$ which in the SMM is understood as the ionization event. For the trajectory passing at $t = T_1$ through $z_s^- = -192.5$ a.u. $t_0 \approx 5T$, i.e., ionization occurs at the maximum strength of the electric field in the Fig. 1 with the field pointing along the forward direction. Electron moves subsequently in the negative $z$ direction, turns

back, and arrives at the detector after forward rescattering, contributing to the maximum of the ionization probability in the forward direction at around 0.01 eV. For the trajectory passing at $t = T_1$ through $z_s^+ = 155$ a.u. the value $t_0 \approx 5.5T$, i.e., the ionization event occurs half a period later when electric field of the pulse in Fig. 1 reaches its secondary maximum. Undergoing the forward rescattering, this trajectory contributes to ionization probability in the backward direction. The SMM does not tell anything, of course, about the relative weights (or probabilities) of these trajectories. Adding to the picture the quantum-mechanical ingredient, the well-known fact [5] that these probabilities grow fast with the electric-field strength at the moment of ionization, we obtain an explanation why Fig. 4 shows that LES around 0.01 eV is much more pronounced in the forward direction.

## III. CONCLUSION

We showed that Gabor transform provides a convenient tool allowing one to gain an insight into the origin of LES. The fully quantum mechanical description used in the work confirms the earlier results that the forward-scattering process plays an important role in forming the LES.The classical trajectories responsible for the LES can be associated with the stationary points of the Gabor transform of the wave function in a natural way. We saw that the location of the stationary points of the Gabor transform very nearly coincides with the values of the $z$ coordinate at the moment of the end of the pulse for which the classical trajectories with near-zero velocity at the moment of the closest approach to the center exists. We saw that this identification is essentially unambiguous, and provides a transparent and, more importantly, quantitatively accurate link between quantum and SMM pictures of the ionization process.

## ACKNOWLEDGMENT

This work was supported by the Institute for Basic Science under Grant No. IBS-R012-D1.

[1] L. V. Keldysh, Sov. Phys. JETP **20**, 1307 (1965).
[2] F. H. M. Faisal, J. Phys. B **6**, L89 (1973).
[3] H. R. Reiss, Phys. Rev. A **22**, 1786 (1980).
[4] A. M. Perelomov, V. S. Popov, and M. V. Terentiev, Sov. Phys. JETP **23**, 924 (1966).
[5] V. S. Popov, Phys. Usp. **47**, 855 (2004).
[6] S. V. Popruzhenko, J. Phys. B **47**, 204001 (2014).
[7] M. V. Ammosov, N. B. Delone, and V. P. Krainov, Sov. Phys. JETP **64**, 1191 (1986).
[8] A. M. Perelomov, V. S. Popov, and M. V. Terentiev, Sov. Phys. JETP **24**, 207 (1967).
[9] V. D. Mur, S. V. Popruzhenko, and V. S. Popov, Sov. Phys. JETP **92**, 777 (2001).
[10] O. I. Tolstikhin and T. Morishita, Phys. Rev. A **86**, 043417 (2012).
[11] M. Lewenstein, P. Balcou, M. Y. Ivanov, A. L'Huillier, and P. B. Corkum, Phys. Rev. A **49**, 2117 (1994).
[12] S. P. Goreslavski and S. V. Popruzhenko, Phys. Lett. A **249**, 477 (1998).
[13] H. B. van Linden van den Heuvell and H. G. Muller, *Multiphoton Processes* (Cambridge University Press, Cambridge, UK, 1987).
[14] C. I. Blaga, F. Catoire, P. Colosimo, G. G. Paulus, H. G. Muller, P. Agostini, and L. F. DiMauro, Nat. Phys. **5**, 335 (2009).
[15] H. H. M. Faisal, Nat. Phys. **5**, 319 (2009).
[16] J. Dura, N. Camus, A. Thai, A. Britz, M. Hemmer, M. Baudisch, A. Senftleben, C. D. Schröter, J. Ullrich, R. Moshammer *et al.*, Sci. Rep. **3**, 2675 (2013).
[17] T.-M. Yan, S. V. Popruzhenko, M. J. J. Vrakking, and D. Bauer, Phys. Rev. Lett. **105**, 253002 (2010).
[18] W. Becker, S. P. Goreslavski, D. B. Milošević, and G. G. Paulus, J. Phys. B **47**, 204022 (2014).
[19] A. Rudenko, K. Zrost, T. Ergler, A. B. Voitkiv, B. Najjari, V. L. B. de Jesus, B. Feuerstein, C. D. Schröter, R. Moshammer, and J. Ullrich, J. Phys. B **38**, L191 (2005).
[20] A. S. Landsman, C. Hofmann, A. N. Pfeiffer, C. Cirelli, and U. Keller, Phys. Rev. Lett. **111**, 263001 (2013).
[21] I. A. Ivanov, Phys. Rev. A **90**, 013418 (2014).
[22] Q. Z. Xia, D. F. Ye, L. B. Fu, X. Y. Han, and J. Liu, Sci. Rep. **5**, 11473 (2015).
[23] I. A. Ivanov, Phys. Rev. A **83**, 023421 (2011).
[24] M. Nurhuda and F. H. M. Faisal, Phys. Rev. A **60**, 3125 (1999).
[25] C. K. Chui, *An Introduction to Wavelets* (Academic Press, Boston, 1992).
[26] X. Chu and S.-I. Chu, Phys. Rev. A **64**, 021403(R) (2001).
[27] X. M. Tong and S.-I. Chu, Phys. Rev. A **61**, 021802(R) (2000).
[28] P. Antoine, B. Piraux, and A. Maquet, Phys. Rev. A **51**, R1750 (1995).
[29] J. Zhao and M. Lein, Phys. Rev. Lett. **111**, 043901 (2013).
[30] M. L. Goldberger and K. M. Watson, *Collision Theory* (John Wiley and Sons, New York, 1964).